Early stages of the Schottky barrier formation in submonolayer Pt on SrTiO_{3} (001)

Hosung Seo and Alexander A. Demkov

Phys. Rev. B **92**, 245301 — Published 4 December 2015

DOI: 10.1103/PhysRevB.92.245301

Early stages of Schottky barrier formation in sub-monolayer Pt on $SrTiO_3$ (001)

Hosung Seo[1] and Alexander A. Demkov[2]

Department of Physics, The University of Texas at Austin, Texas 78712, USA

We investigate the early stages of Pt nano-cluster formation on $SrTiO_3$ (001) and the emergence of the Schottky barrier at the interface as a function of sub-monolayer Pt coverage using density function theory. We find that there is a critical coverage of 3/8 monolayer (ML), below which the Pt–oxide interaction is dominant, leading to an ordered reconstructed surface with local Pt(II) oxide structures. Beyond the critical coverage of 3/8 ML, the system undergoes a crossover when the Pt-Pt interaction becomes dominant, starting to develop a closed-pack hexagonal Pt nano-clusters. We show that cluster-induced gap states emerge along with the crossover and pin the Fermi level at 1.3 eV above the valence band edge, thus playing a critical role in determining the Schottky barrier height of the Pt/$SrTiO_3$ (001) interface.

I. INTRODUCTION

Noble metal nano-clusters on oxide substrates attracted a significant amount of attention for their interesting electronic and structural properties [1-4] as well as their critical roles in technological applications such as photo-catalysis [5-7]. $SrTiO_3$ (STO) has been identified as a photo-catalyst for hydrogen production using water splitting under zero bias [8-11]. The band gap of STO is 3.2 eV (UV-active) and the conduction band minimum is positioned about 4.0 eV below the vacuum level, matching to the redox properties of water molecules [12]. However, the overall quantum efficiency is low and a number of limiting factors have been intensively discussed in the

[1] Current address: The Institute for Molecular Engineering, The University of Chicago, Chicago, IL 60637
[2] demkov@physics.utexas.edu

literature [12,13]. In particular, a major challenge is to decrease the electron-hole recombination rate after they are created under a light irradiation. A possible solution to this problem is designing a suitable heterogeneous catalyst to separate electrons and holes at the interface. Noble metals, such as Pt, are frequently loaded on titania as a co-catalyst to boost the catalytic activity of titania [8,14-18]. The enhanced catalytic activity has been in part attributed to the fact that Pt on STO forms a Schottky barrier [19-24] and the rectifying behavior of the Schottky barrier may allow Pt nano-clusters on the oxide surface to trap electrons, which could effectively reduce the oxidants in a photocatalytic process [12,25]. However, while the interfacial electronic structure seems to play an important role in boosting the photocatalytic activity of Pt nano-clusters/STO, the formation of the interface and the Schottky barrier is not well understood.

In this paper, we use density functional theory (DFT) to investigate the early stages of Schottky barrier formation occurring in sub-monolayer Pt on the $SrTiO_3$ (001) surface. A crucial step for understanding the Schottky barrier of a metal-oxide system is to identify the character of the interface states responsible for charge transfer and thus the formation of a dipole layer at the interface [23,26]. Interestingly, previous photoemission studies on the Pt-STO system as a function of Pt coverage indicated that the Schottky barrier formation is a rather continuous process [19-22], meaning that Pt-related interface states appear at the Fermi level and evolve even at a sub-monolayer coverage of Pt, and a sharp metallic feature at the Fermi level settles in at around the full monolayer coverage. It is worth noting that a similar continuous process of barrier formation has been explored in a number of sub-monolayer metal/semiconductor interfaces experimentally [27,28] and theoretically [29,30]. The character of the interface-induced gap states mediating interfacial charge transfer could be largely dependent on the

dominant interaction at the interface, and thus interfacial morphology. A limiting case is when a metallic over-layer wets an oxide surface, and a metal-oxygen interaction dominates the electronic and chemical interactions at the interface. In this case, charge transfer and thus the Schottky barrier at the interface, can be mainly determined by considering the metal-oxygen chemical bonds [31]. An opposite limiting case is when metal-metal interactions dominate and metal-oxide interactions are relatively weak or negligible. Then, in the case of Pt, it is natural to consider a formation of metallic fcc nanocrystals on the surface. The Fermi level of the metallic *d*-band would be pinned by the charge neutrality level of the oxide [24, 32].

Several DFT calculations have been performed to address the interface and Schottky barrier formation at the Pt/STO(001) interface [23,33-35]. Asthagiri and Sholl explored the favored arrangement of a Pt(001) monolayer on TiO_2-terminated STO(001) and found that Pt(001) prefers to absorb on top of the oxygen sites, suggesting a coherent epitaxial Pt/STO(001) interface up to 5 Pt monolayers [33]. Mrovec *et al.* adopted the Pt/STO(001) structure suggested by Asthagiri and Sholl and calculated its *p*-type Schottky barrier to be 1.8 eV [23]. We note, however, that the (001) orientation of a Pt overlayer, which was the main assumption in the previous studies [23,33] may not be the most likely structure of Pt on STO(001), and a disordered (111)-type Pt overlayer is more likely to occur based on our recent results [34,35]. It is also worth mentioning that researchers found interesting kinetics of Pt sub-monolayer on a number of different oxide surfaces such as TiO_2 [36-38]. Therefore, a detailed study on the structural property and its effect on the emergence of in-gap states in a sub-monolayer of Pt on STO may provide a deeper understanding of the Schottky barrier formation of dispersed Pt nano-particles on STO.

For the Pt/STO (001) system, Christensen *et al.*, reported interesting hierarchical nanoparticle morphology [39], where Pt at around one monolayer coverage aggregated to well-dispersed nanoparticles, but without coalescence [39]. It is intriguing, because thermodynamically, Pt would prefer to completely coalesce to minimize the Pt surface area, as the surface energy of Pt is much higher than that of STO (001) [34,35]. It was argued that there might be some mechanisms, which kinetically hinder the thermodynamic forces through a chemical state of Pt or a physical barrier at a low Pt coverage [39]. This hierarchical Pt nanoparticle morphology is certainly beneficial to photocatalytic applications, because the system could maintain a high surface-to-volume ratio. On the other hand, a subtle competition between Pt-Pt interaction and Pt-surface interaction might exist at a low coverage of Pt. Using atomic layer deposition (ALD) and X-ray absorption spectroscopy (XAS), Christensen *et al.* have observed an evolution from Pt(II) oxide to metallic Pt and an increase in Pt-Pt bonding with a decrease in Pt-O bonding in the early stages of sub-monolayer Pt deposition [40].

To elucidate the subtle interplay between the Pt-Pt and Pt-STO interactions and its consequence on the Schottky barrier formation in the sub-monolayer Pt/STO system, we theoretically investigate the early stages of Pt growth on TiO_2-terminated STO (001) and the emergence of in-gap states in the sub-monolayer Pt on that surface. The paper is organized as follows. In section II, we summarize our computational methods. We present our main results in section III, in which we discuss about the behavior of Pt monomer, dimer and trimer on the TiO_2-terminated STO(001) surface. In section IV, we summarize our main conclusions and discuss about the

possible connections between our theoretical results and the existing experimental results in the literature.

II. COMPUTATIONAL DETAILS

We use density functional theory within the local density approximation as implemented in the VASP code [41]. The exchange-correlation functional is approximated using the parameterization of Ceperley-Alder data by Perdew and Zunger [42]. We employ projector augmented wave pseudopotentials to describe Sr, Ti, O, and Pt [43] and cutoff energy of 600 eV is used. Valence electron configurations for the elements are $4s^2 4p^6 5s^2$ for Sr, $3d^2 4s^2$ for Ti, $2s^2 2p^4$ for O, and $5d^9 6s^1$ for Pt. Each self-consistent electronic calculation is converged within 10^{-6} eV/cell and the ionic relaxation is performed until the forces are less than 0.01 eV/Å. We use a supercell method to investigate the interaction between sub-monolayer Pt and STO (001). We model the TiO_2-terminated STO(001) surface using a 4 unit-cell thick STO slab with a 2×2 surface cell (lateral dimension of 7.75 Å × 7.75 Å). The STO (001) slab in the supercell is separated by 16 Å thick vacuum space from its next nearest periodic images to avoid a spurious slab-slab interaction. For the ionic relaxation, we use a 4×4×1 *k*-point grid. For selected configurations of 1/8 and 1/4 monolayer (ML) coverage of Pt on STO, we check that the main results remain unchanged as we change the cutoff energy and the *k*-point grid to 700 eV and 6×6×2, respectively. For the density of state (DOS) and total energy calculation, we use the 6×6×2 *k*-point grid. To satisfy the periodic boundary condition along the *c*-direction, the bottom STO surface is reconstructed in the same way as the top STO surface is. In other words, there is a mirror plane at the center of each supercell and this is also essential to properly describe the interfacial electronic structure.

III. RESULTS

1. Potential energy surface for one Pt atom on STO (001)

We start our investigation by considering 1/8 ML coverage of Pt on the STO surface. This corresponds to one Pt on the 2×2 surface. Pt-Pt bond length in the Pt bulk is 2.763Å in our theory. Therefore the (2×2) surface is large enough, allowing us to consider the Pt ad-atom as a separate entity on the surface. We calculate the potential energy surface (PES) for one Pt ad-atom and it is shown in Fig. 1 (a).

From the PES in Fig. 1 (a), we note that Pt can be bound by surface O while Ti repels it. We also see that the O sites provide relatively shallow local minima, but Pt feels much stronger and deeper potential at the hollow site where Pt is maximally coordinated by four oxygen atoms on the surface. The energy barrier from the hollow site to the nearest O site is calculated to be 2.04 eV, while the barrier between the nearest neighboring O sites is 0.46 eV. To estimate the time scale for Pt diffusion, we use the Arrhenius formula for kinetics, $1/\tau = \nu e^{-E/k_B T}$, where τ is a time interval between Pt hopping, E is the energy barrier for hopping, and υ is an attempt frequency [44]. Assuming $\upsilon \approx 10^{12}$ sec^{-1}[45], the time scales for hopping at room temperature are on the order of microseconds and 10^{22} seconds for the case of the O site to the O site and that of the hollow site to the O site, respectively. Therefore, a Pt ad-atom is highly mobile on the most of the STO (001) surface area, but if Pt is trapped at the hollow site, it cannot escape by itself.

Interestingly, Pt captured at the hollow site not only maximizes the coordination number by O, but also sinks down into the surface as shown in Fig. 1(b), forming PtO-like local oxide structure in a square-planar geometry [40,46-48]. In Fig. 1 (c), we plot the projected density of states of

the surface TiO_2 layer with adsorbed Pt. It is clearly seen that 5-fold degenerate atomic *d* states of Pt split and resonate in energy with surface O 2*p* states due to the bonding interaction. In Fig. 2, we show some of these bonding and anti-bonding orbitals. We find the Pt-O bond length to be 2.01 Å that is close to 2.04 Å of the PtO bulk [46,47] and to 1.98 Å of PtO formed on the STO(001) surface [40]. We calculate the amount of charge transfer from Pt to O using the Bader charge analysis [49,50], to be 0.83*e* that is also close to 0.86*e* in bulk PtO [48] In the presence of the PtO structure, the surface stoichiometry is $PtTi_4O_8$. Assuming the nominal oxidation state of 2+ for Pt in PtO, Ti on the reconstructed surface would have the oxidation state of 3.5+. This feature gives rise to a metallic surface due to the partial occupation of the bottom of the conduction band originating from the Ti 3d t_{2g}* states, as shown in Fig. 1 (c). We will call this surface $PtTi_4O_8$ or PTO for the rest of this paper.

2. Pt clusters

Next, we consider the interaction between additional Pt atoms on the reconstructed PTO surface. We first check that if there is a Pt_2 dimer on the clean STO (001) surface, it is energetically favorable to break the dimer bond and form the two local PtO structures separated by a hollow site. In Fig. 3 we plot the PES for a second incoming Pt on the PTO surface. A noticeable feature is that the nearest neighbor hollow sites of a PtO structure do not bind the second Pt atom. It means that at the Pt coverage of 1/8 ML the TiO_2 surface is fully saturated by the local PtO structures. It is also interesting that the PtO structures provide large kinetic barriers for the Pt diffusion. In addition to the enormous barrier around the hollow site trapping a Pt atom, crossing the barrier present between the local PtO structures requires 390 meV as shown in Fig. 3. In addition, we remark that now the Ti sites are able to bind Pt, which was not possible on the clean STO(001) surface as shown in Fig. 1(a). The Pt-Ti binding is a metallic bond and it is possible as

Ti in the PTO surface have partial electron occupation (see Fig. 1 (c)). Setting the binding energy of Pt on the O site to be 0.0 meV, the binding energy of Pt on the Ti site is only 6 meV higher in energy and the diffusion barrier between the O and Ti sites are calculated to be 78 meV as shown in Fig. 3.

To find the lowest energy Pt nanostructure at the coverage of 3/8 ML, we consider 25 different initial configurations of Pt based on the low energy structures from the 2/8 ML Pt configurations. We first consider all possible configurations of dispersed Pt atoms adsorbed on top of the O and Ti sites that are identified as the binding sites of the PES in Fig. 3. However, there is always 3~5 eV energy gain when Pt dimerizes in the square potential well shown in Fig. 3. We show the lowest energy Pt dimer structure on the PTO surface in Fig. 4 (a). The Pt-Pt bond length is calculated to be 2.47 Å that agrees with a theoretical bond length of Pt dimer of about 2.4 Å in a gas phase [51]. Next, we consider Pt trimer on the clean TiO_2 surface and the lowest energy structure is shown in Fig. 4 (b). Interestingly, there is an energy gain of 150 meV, compared to that in the Fig. 4 (a). We also check that if the Pt dimer in Fig. 4 (a) is brought on top of the PtO structure, then subsequent structural relaxation destabilizes the PtO structure and a Pt trimer is formed on the surface. We note that Pt_3 no longer follows the surface symmetry as shown in Fig. 4 (b). Instead, it has a triangular structure, which is a motif of a closed-pack hexagonal structure of the Pt (111) layer. We calculate the bond lengths and angles to be varying from 2.47 to 2.55 and from 59 to 62 degrees, respectively, that closely follows the Pt trimer structure in a gas phase [51]. The trimer structure is also not planar on the surface because the Ti site now tends to repel Pt on top of it.

In Fig. 5 (a) and (b), we show atom-projected density of states calculated using the structures shown in Fig. 4 (a) and (b), respectively. We note that structural transition from the dimer in Fig. 4 (a) to the trimer structure in Fig. 4 (b) is driven by the stronger metallic Pt-Pt interaction in the Pt trimer [51] than the Pt-oxide interaction mediated by the surface oxygen. Comparing Fig. 5 (a) and (b), we observe that the structural transition creates a significant number of states near the Fermi level in the band gap of STO. Our results show that interface-induced states in the STO gap start to appear even at the sub-monolayer Pt coverage and metallicity in the Pt nano-clusters also start to develop as manifested by the appearance of the large metallic *d*-band-like DOS below the Fermi level. By considering the pDOS of the middle STO layer of the cell (not shown), we find that the Fermi level is pinned at 1.3 eV above the STO valence band top, which is the same as the charge neutrality of STO calculated by Demkov *et al.* using the complex band structure of STO [32]. We will further show that the Fermi level of a full monolayer Pt – STO (001) structure is also pinned at 1.3 eV above the STO valence band top. The Fermi level pinning for the Pt_3 trimer is intriguing because the Pt_3 trimer is not truly metallic with a full metallic *d*-band by itself. The minimum distance between the Pt trimer and it nearest neighbor image trimer in Fig. 4 (b) is 5.3 Å, meaning that the direct Pt trimer – trimer interaction is negligible. So, technically speaking, they are cluster-induced gap states. It is also very interesting to see that the states near the Fermi level in the STO gap have the orbital character of both Ti and O. We note that the evanescent states in the gap change their character from the valence-like to the conduction-like as a function of the Fermi level position in the gap. Therefore, since the Fermi level is pinned at the branch point of the complex band, which is the charge neutrality level, the states at the Fermi level have both the conduction (mostly Ti 3*d*-states) and the valence (mostly O 2*p*-states) character as shown in Fig. 5 (b).

To calculate the Schottky barrier of a full Pt monolayer on STO (001), we consider a number of Pt (001) and Pt(111) monolayer geometries on STO(001). We find the lowest energy structure of a monolayer Pt(001) configuration is one, in which all the Pt atoms are bound by the surface oxygen atoms [34], which is consistent with previous calculations [33]. To consider Pt(111) on STO(001), we use a $\sqrt{2}a \times 2\sqrt{2}a$ surface cell (Fig. 6(a)), where a is the STO lattice constant. After matching Pt(111) to the surface cell, we translate the Pt(111) sheet over the surface and find the lowest energy structure, which is shown in Fig. 6 (a). We note that there is a small lattice mismatch between Pt and STO of 0.9% in theory and 0.5% in experiment. So, the Pt(111) sheet shown in Fig. 6 (a) is slightly strained along the *b*-direction and it is free to relax in the *a*-direction. In addition, the Pt(111) sheet should be free to rotate in principle, but it is not allowed in our calculations due to the surface cell size and the periodic boundary condition. We argue, however, that the dominant interaction at the full monolayer Pt coverage would be the Pt-Pt metallic interaction as discussed for the Pt_3 trimer structure on STO. Therefore, the Pt(111) structure that is considered in Fig. 6 (a) would capture the essential feature of the interfacial electronic structure and charge transfer property through the metal induced gap states in STO.

We first note that the energy of the Pt(111) structure shown in Fig. 6(a) is lower than that of the lowest Pt(001) structure by 0.43eV per Pt atom. This is consistent with our previous conclusion that beyond the 3/8ML Pt coverage Pt nano-clusters on STO(001) do not follow the surface (1×1) symmetry but prefer to form Pt(111) hexagonal structures. We show the layer-by-layer pDOS of the Pt(111)/STO(001) system in Fig. 6(b). We observe that the monolayer Pt(111) sheet exhibits a full metallic *d*-band and it transfers electrons to the evanescent gap states in STO. Additionally,

the charge transfer rapidly decays within the two unit-cells of STO and the bulk electronic structure of STO is recovered in the middle of the supercell, which is consistent with the complex band structure calculations [32]. We calculate the Fermi level is pinned at 1.3eV above the valence band top, which is the same for the Pt_3 cluster on STO(001) as shown in Fig. 5(b). By considering the experimental STO band gap of 3.2eV, we calculate the *n*-type Schottky barrier height between the Pt(111) sheet and STO(001) to be 1.9 eV. Our results suggest that the Fermi level pinning, thus the emergence of the Schottky barrier in the Pt nano-cluster/STO system is controlled by the evanescent states of the bulk STO and it appears when the Pt-Pt metallic interaction becomes dominant over the Pt-surface interaction, which is consistent with the previous experimental observations [19,40].

IV. DISCUSSIONS AND CONCLUSION

In conclusion, we have theoretically investigated the early stages of the interface and Schottky barrier formation in sub-monolayer Pt on $SrTiO_3$ (001). We found that there is a drastic change in the binding mechanism of Pt on STO as a function of Pt coverage. At a low coverage below 2/8ML, the dominant interaction is Pt-O chemical bonding interaction while Ti sites repel Pt, leading to the formation of local Pt(II) oxide structures on the surface. In the presence of the local PtO structures, however, the Ti sites are able to bind Pt through a metallic bonding. Upon increasing the Pt coverage, metallic Pt-Pt interaction becomes dominant and hexagonal Pt(111) nanocrystals start to form, making the interaction between Pt and the oxide to be neither directional nor site-specific. We note that our finding is consistent with the experimental results reported by Christensen *et al.*, who used atomic layer deposition and X-ray absorption spectroscopy and observed a progression from Pt(II) oxide to metallic Pt as the Pt coverage on STO(001) is increased [40]. Additionally, our results indicated that at a low coverage of Pt on

STO(001), the local PtO structures can provide kinetic barriers, which may play a role to hinder the complete coalescence of Pt nanostructure and help retain high surface-to-volume ratio [39]. This high surface-to-volume ratio should be advantageous for low-coverage Pt on STO to be used as an efficient photo-catalyst.

We show that the formation of the Schottky barrier is a continuous process [19-22]. We found that interface-induced gap states pinning the Fermi level start to appear in the STO band gap even at sub-monolayer Pt coverage and the emergence of the gap states is directly associated with the change in the dominant interaction on the surface. We also show that at a coverage below 3/8ML of Pt, the dominant Pt-O chemical bonding, which drives the formation of local Pt(II) oxide structure controls the Fermi level position. However, above the critical coverage of 3/8ML, the interface starts to develop interface-induced gap states as Pt-Pt metallic interaction starts to dominate and Pt prefers to develop (111) hexagonal nanocrystals. The cluster-induced gap states pin the Fermi level 1.3 eV above the STO valence band top. We also show that the Fermi level of a full metallic Pt(111) monolayer is pinned at the same energy by the same evanescent metal-induced gap states (MIGS). Based on the MIGS theory, the STO pinning factor S is 0.28 using the dielectric constant of STO [24], suggesting a moderate Fermi level pinning at metal/STO interfaces. Therefore, our result suggests that the pinning level of 1.3 eV at the Pt/STO(001) interface is close to the charge neutrality level of STO, which is consistent with the estimate of Demkov *et al.* [32].

We calculate the *n*-type Schottky barrier of the Pt/STO(001) interface to be 1.9 eV by subtracting the *p*-type Schottky barrier of 1.3 eV from the experimental band gap of STO, which is 3.2 eV.

We use the experimental band gap as the theoretical value is only 1.7 eV, due to the well-known band gap underestimation inherent to (semi-)local exchange-correlation functionals such as LDA or GGA [52]. The application of higher-level theories such as GW many-body perturbation theory [53] or properly tuned Hartree-Fock hybrid functional theory [54] to Pt/dielectric oxide systems [55] may result in improved prediction of the *n*-type Schottky barrier heights of these and related heterogeneous photo-catalytic systems. We also emphasize the importance of an explicit interface calculation as the detailed structure of the interface controls the charge transfer, thus the charge neutrality level and the pinning strength in the MIGS theory.

We also note that there are unresolved issues about the Schottky barrier formation at the Pt/STO(001) interface, which we left for future study. For example, we calculated the *p*-type Schottky barrier height of the meta-stable Pt(001) overlayer on STO(001) to be 1.8 eV and this is in a good agreement with the previous results of Mrovec *et al.* [23]. Experimentally, Schafranek and co-workers [19] measured the *n*-type Schottky barrier heights for the $SrTiO_3$:Nb/Pt interface to be 1.5 eV and 0.6 eV for the oxidized and reduced interface, respectively, which are converted to 1.7 eV and 2.6 eV *p*-type Schottky barrier heights by using the 3.2 eV band gap of STO. It seems that the experimental value of 1.7 eV for the oxidized interface is in a good agreement with the theoretical result of 1.8 eV that is obtained from the meta-stable epitaxial Pt(001) overlayer on STO(001). We note, however, that this does not necessarily mean that the Pt(001) overlayer is the structure observed in experiment, but the situation could be more complex [19], which we will further investigate in the future.

ACKNOWLEDGEMENT

We thank Agham Posadas for critical reading the manuscript and helpful discussions. H.S. gratefully acknowledges a support from the University of Texas at Austin through William Powers, Jr. Presidential Fellowship. A.D. is grateful for support by the Air Force Office of Scientific Research under grant FA9550-12-10494.

REFERENCE

[1] F. Silly and M. R. Castell, Phys. Rev. Lett. **96**, 086104 (2006).

[2] N. Nilius, M. V. Ganduglia-Pirovano, V. Brázdová, M. Kulawik, J. Sauer, and H.-J. Freund, Phys. Rev. Lett. **100**, 096802 (2008).

[3] Z. Novotný, G. Argentero, Z. Wang, M. Schmid, U. Diebold, and G. S. Parkinson, Phys. Rev. Lett. **108**, 216103 (2012).

[4] Q. Fu and T. Wagner, Surf. Sci. Rep. **62**, 431 (2007).

[5] M. S. Chen and D. W. Goodman, Science **306**, 252 (2004).

[6] G. N. Vayssilov *et al.*, Nat. Mater. **10**, 310 (2011).

[7] M. Kitano, K. Tsujimaru, and M. Anpo, Top. Catal. **49**, 4 (2008).

[8] R. G. Carr and G. A. Somorjai, Nature **290**, 576 (1981).

[9] F. T. Wagner, S. Ferrer and G. A. Somorjai, Surface Science **101**, 462 (1980).

[10] F. T. Wagner and G. A. Somorjai, J. Amer. Chem. Soc. **102**, 5494 (1980).

[11] F. T. Wagner and G. A. Somorjai, Nature **285**, 559 (1980).

[12] X. Chen, S. Shen, L. Guo, and S. S. Mao, Chem. Rev. **110**, 6503 (2010).

[13] M. R. Hoffman, S. T. Martin, W. Y. Choi, D. W. Bahnemann, Chem. Rev. **95**, 69 (1995).

[14] A. Paracchino, V. Laporte, K. Sivula, M. Grätzel, and E. Thimsen, Nat. Mat. **10**, 456 (2011).

[15] S. Ikeda et al., Catal. Today **117**, 343 (2006).

[16] B. Sun, a. V. Vorontsov, and P. G. Smirniotis, Langmuir **19**, 3151 (2003).

[17] J. A. Enterki, K. R. Poeppelmeier, and L. D. Marks, Nano Lett. **11**, 993 (2011).

[18] J. A. Enterkin, W. Setthapun, J. W. Elam, S. T. Christensen, F. A. Rabuffetti, L. D. Marks, P. C. Stair, K. R. Poeppelmeier, and C. L. Marshall, ACS Catal. **1**, 629 (2011).

[19] R. Schafranek, S. Payan, M. Maglione, and A. Klein, Phys. Rev. B **77**, 195310 (2008).

[20] M. Copel, P. R. Duncombe, D. A. Neumayer, T. M. Shaw and R. M. Tromp, Appl. Phys. Lett. **70**, 3227 (1997).

[21] Y. W. Chung and W. B. Weissbard, Phys. Rev. B 20, 3456 (1979).

[22] M. K. Bahl, S. C. Tsai, and Y. W. Chung, Phys. Rev. B **21**, 1344 (1980).

[23] M. Mrovec, J.-M. Albina, B. Meyer, and C. Elsässer, Phys. Rev. B **79**, 245121 (2009).

[24] J. Robertson and C. W. Chen, Appl. Phys. Lett. **74**, 1168 (1999).

[25] J. S. Jang, H. G. Kim, and J. S. Lee, Catal. Today **185**, 270 (2012).

[26] M. K. Niranjan, L. Kleinman, and A. A. Demkov, Phys. Rev. B **77**, 155316 (2008).

[27] M. Prietsch, M. Domke, C. Laubschat, and G. Kaindl, Phys. Rev. Lett. **60**, 436 (1988).

[28] K. Stiles and A. Kahn, Phys. Rev. Lett. **60**, 440 (1988).

[29] A. Zunger, Phys. Rev. B **24**, 4372 (1981).

[30] J. Ortega and F. Flores, Phys. Rev. Lett. **63**, 2500 (1989).

[31] R. T. Tung, Phys. Rev. Lett. **84**, 6078 (2000).

[32] A. A. Demkov, L. R. C. Fonseca, E. Verret, J. Tomfohr, and O. F. Sanky, Phys. Rev. B **71**, 195306 (2005).

[33] A. Asthagiri and D. S. Sholl, J. Chem. Phys. **116**, 9914 (2002).

[34] H. Seo, A. B. Posadas, and A. A. Demkov, J. Vac. Sci. Technol. B **30**, 04E108 (2012).

[35] K. D. Fredrickson, A. B. Posadas, A. A. Demkov, C. Dubourdieu and J. Bruley, J. Appl. Phys. **113**, 184102 (2013).

[36] H. Iddir, S. Öğüt, N. D. Browning, and M. M. Disko, Phys. Rev. B **72**, 081407(R) (2005).

[37] H. Iddir, V. Skavysh, S. Öğüt, N. D. Browning, and M. M. Disko, Phys. Rev. B **73**, 41403(R) (2006).

[38] T. Chang, Y. Tanaka, R. Ishikawa, K. Toyoura, K. Matsunaga, Y. Ikuhara, and N. Shibata, Nano Lett. **14**, 134 (2014).

[39] S. T. Christensen, B. Lee, Z. Feng, M. C. Hersam, M. J. Bedzyk, Appl. Surf. Sci. **256**, 423 (2009).

[40] S. T. Christensen, J. W. Elam, F. A. Rabuffetti, Q. Ma, S. J. Weigand, B. Lee, S. Seifert, P. C. Stair, K. R. Poeppelmeier, M. C. Hersam, M. J. Bedzyk, Small **5**, 750 (2009).

[41] G. Kresse and J. Furthmüller, Phys. Rev. B. **54**, 11169 (1996).

[42] J. P. Perdew and A. Zunger, Phys. Rev. B **23**, 5048 (1981).

[43] P. E. Blöchl, Phys. Rev. B **50**, 17953 (1994).

[44] H. Brune, Surf. Sci. Rep. **31**, 125 (1998).

[45] L. Xy, G. Henkelman, C. T. Campbell, H. Jonsson, Surf. Sci. **600**, 1651 (2006).

[46] W. J. Moore and L. Pauling, J. Am. Chem. Soc. **63**, 1392 (1941).

[47] J. R. McBride, G. W. Graham, C. R. Peters, and W. H. Weber, J. Appl. Phys. **69**, 1596 (1991).

[48] N. Seriani, Z. Zin, W. Pompe, and L. C. Ciacchi, Phys. Rev. B **76**, 155421 (2007).

[49] R. F. W. Bader, *Atoms in Molecules: A Quantum Theory* (Oxford University Press, Oxford, 1990).

[50] W. Tang, E. Sanville, and G. Henkelman, J. Phys.: Condens. Matter **21**, 084204 (2009).

[51] P. Bloński, S. Dennler, J. Hafner, J. Chem. Phys. **134**, 034107 (2011).

[52] J. P. Perdew and M. Levy, Phys. Rev. Lett. **51**, 1884 (1983).

[53] M. Govoni and G. Galli, J. Chem. Theory Comput. **11**, 2680 (2015).

[54] J. H. Skone, M. Govoni, and G. Galli, Phys. Rev. B **89**, 195112 (2014).

[55] C. Cazorla and M. Stengel, Phys. Rev. B **85**, 075426 (2012).

FIGURE CAPTIONS

Figure 1. (Color online) (a) Potential energy surface (PES) for a Pt ad-atom on the $2a \times 2a$ STO surface, where a is the STO lattice constant. The lowest energy is set to 0 eV. The spatial resolution is 0.48 Å. (b) The lowest energy structure for the 1/8 ML coverage of Pt on STO (001). (c) Projected density of states of the $PtTi_4O_8$ surface layer shown in (b). The Fermi energy (E_F) is shown as a dashed vertical line.

Fig. 2. (Color online) The orbital-projected Pt density of states (a) and density plots of bonding and anti-bonding states between Pt 5*d* and O 2*p* orbitals (b) of the $PtTi_4O_8$ surface shown in Fig. 1.

Figure 3. (Color online) The potential energy surface (PES) for Pt on the PTO surface (see Fig. 1 (b)). The size of the PES plot is $4a \times 4a$, where a is the STO lattice constant A schematic of the surface structure is drawn under the PES. The spatial resolution for the PES calculation is 0.96Å.

Saturation level for the plot is set to 1.0 eV, above which the PES is not shown (plateau areas around the Pt sites).

Figure 4. (Color online) Low energy surface structures for 3/8 ML coverage of Pt on STO (001). Pt dimer on the reconstructed PTO surface (a) and Pt trimer on the TiO_2 surface (b). The STO structure below the surface TiO_2 layer is not shown for clarity. The surface unit cell is indicated by dashed line. The upper (lower) picture is a top (side) view.

Figure 5. (Color online) Atom-projected density of states of Pt dimer on the PTO surface (a) and Pt trimer on the TiO_2 surface (b). The upper panels are for adsorbed Pt dimer (a) or trimer (a) and the surface electronic structures are shown in the lower panels. The Fermi energy is set to 0 eV.

Figure 6. (Color online) (a) Schematic of a full monolayer of Pt(111) on the TiO_2-terminated STO(001) surface viewed from the top (up) and the side (bottom). The top TiO_2 layer and the Pt(111) sheet are only visible in the top view for clarity. (b) The layer-by-layer projected density of states of the Pt(111)/STO(001) structure. The Fermi level is pinned at 1.3 eV above the valence band top of the bulk STO.

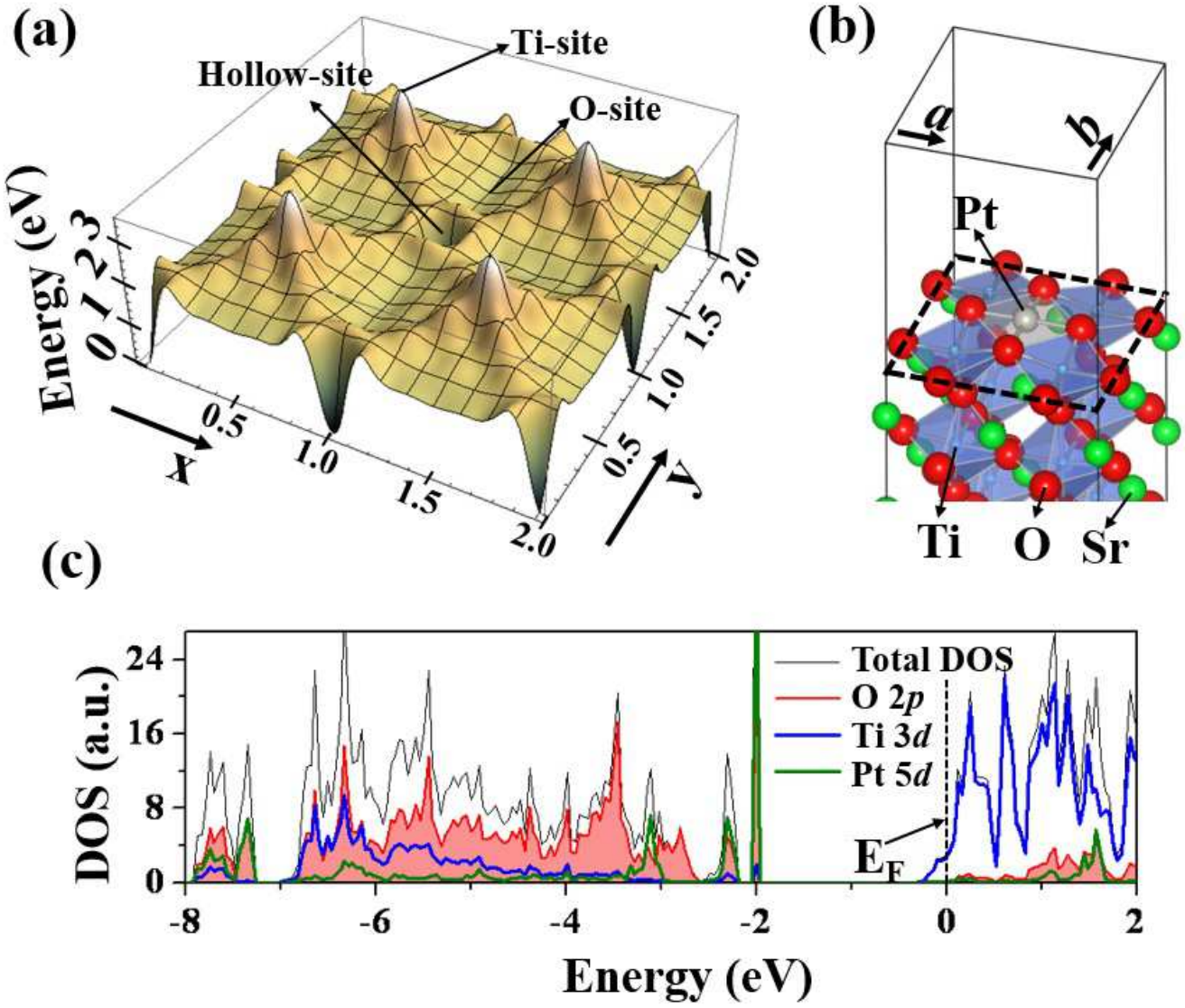

Figure 1 BJ12801 03NOV2015

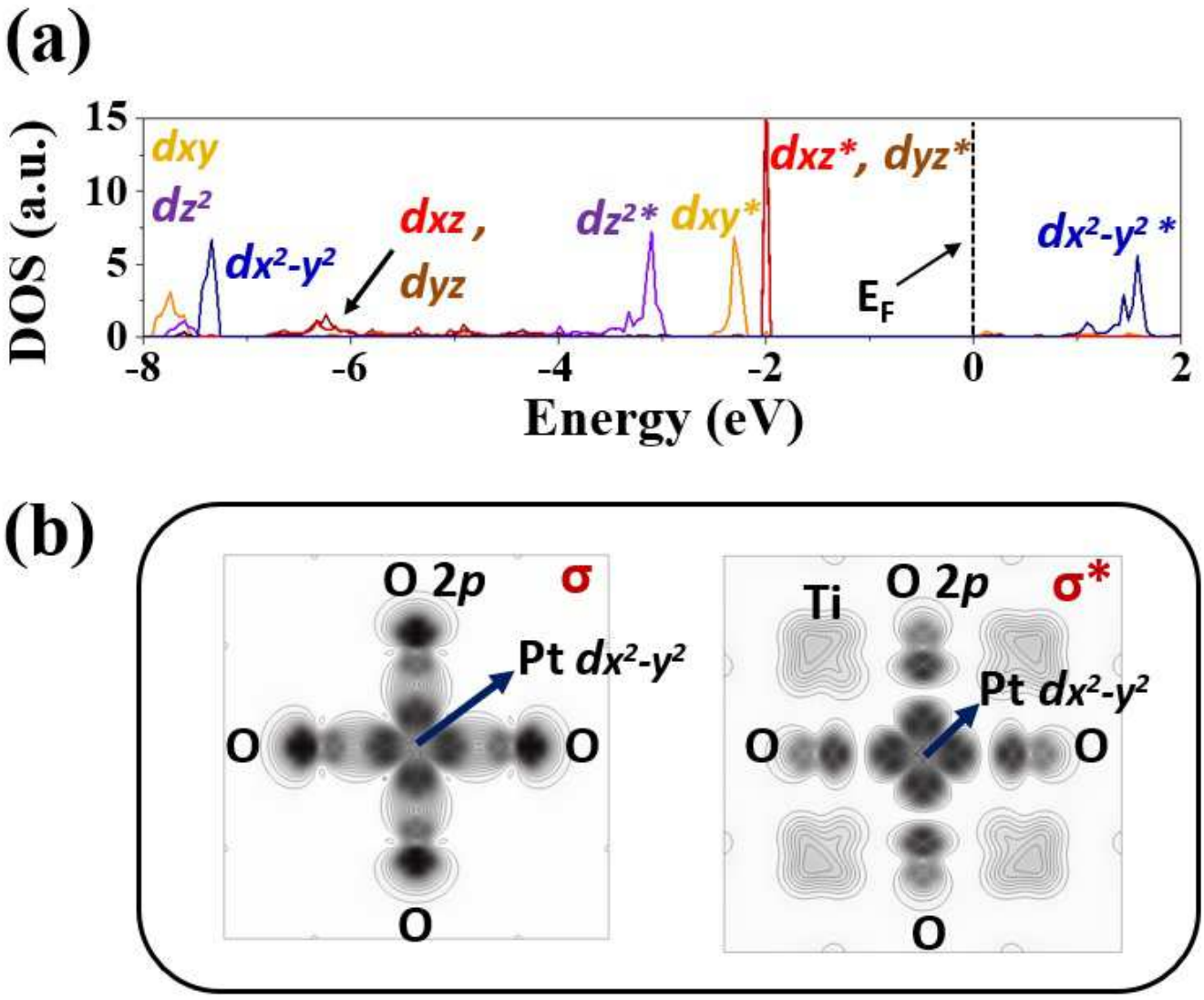

Figure 2 BJ12801 03NOV2015

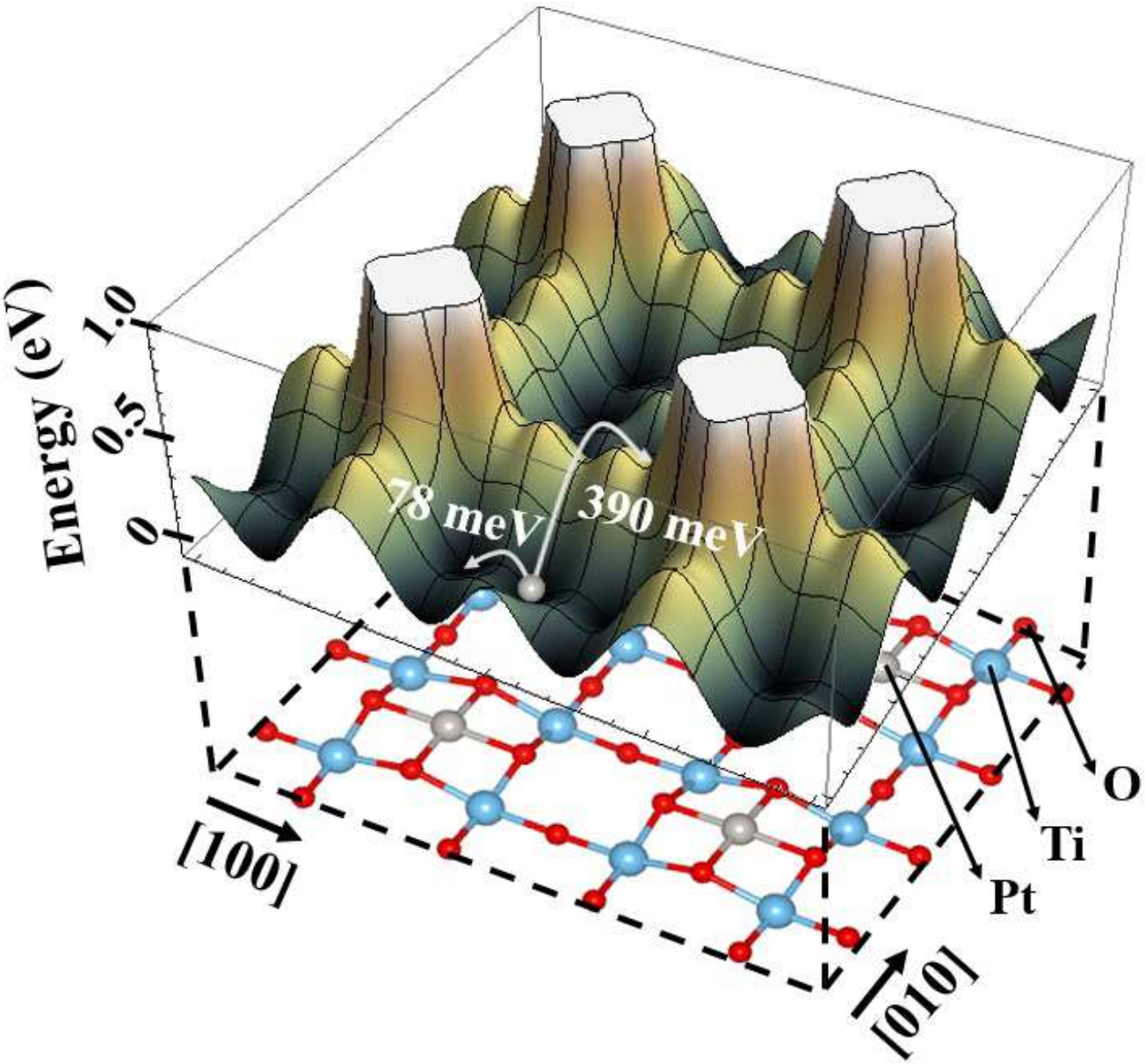

Figure 3 BJ12801 03NOV2015

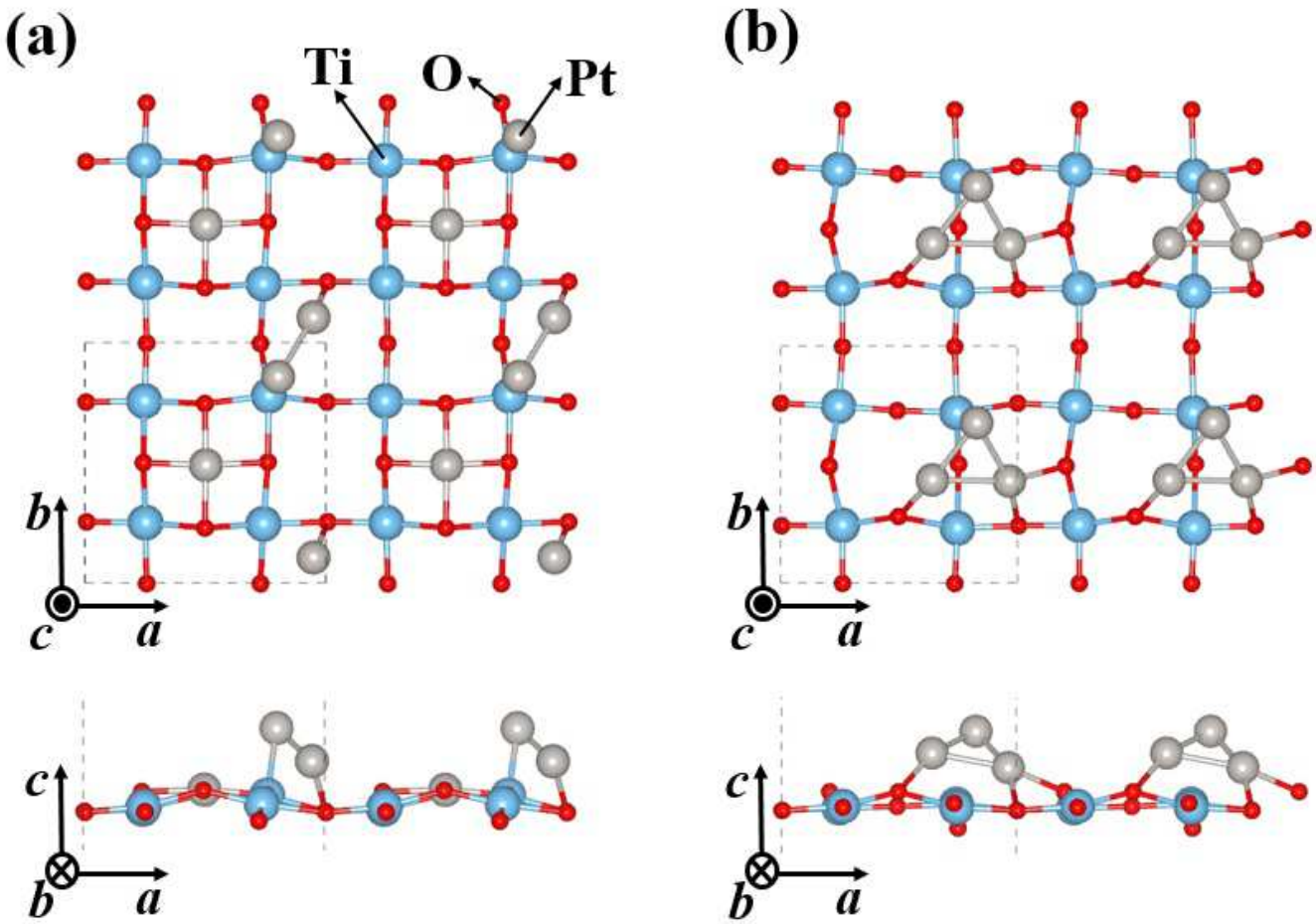

Figure 4 BJ12801 03NOV2015

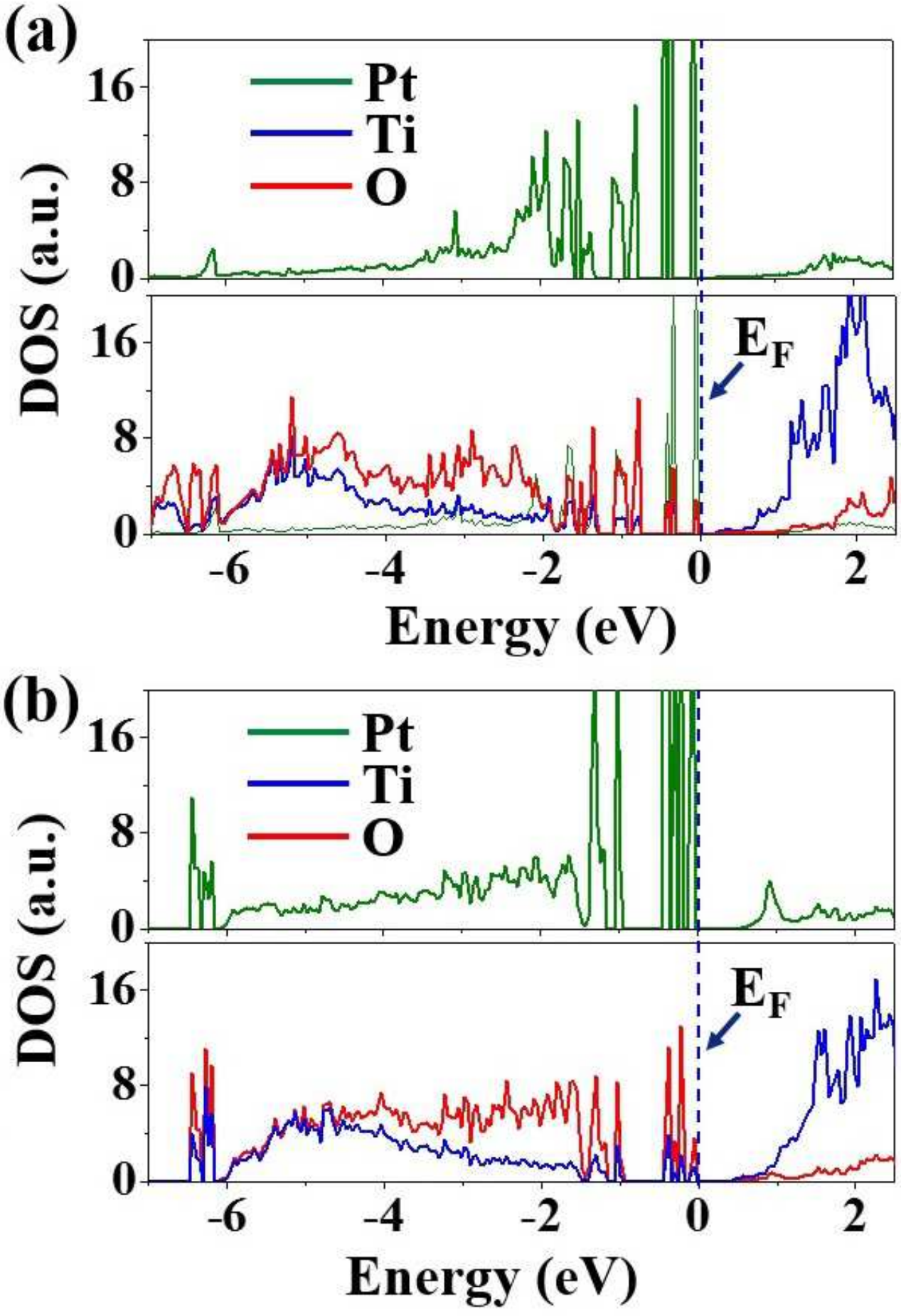

Figure 5 BJ12801 03NOV2015

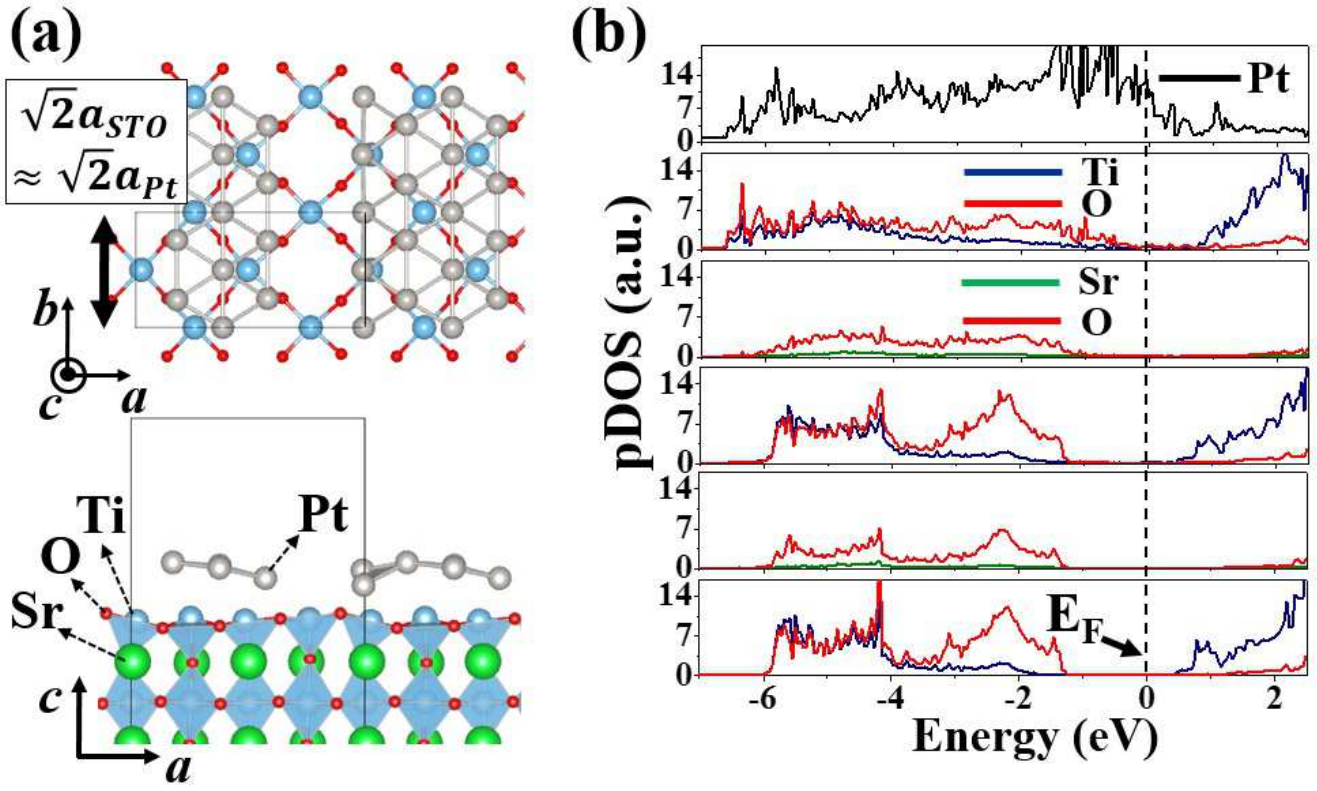

Figure 6 BJ12801 03NOV2015